PAPER

Check for updates

Solid-state reduction of silica nanoparticles via oxygen abstraction from SiO4 units by polyolefins under mechanical stressing†

Mamoru Senna, [ID] *[ab] Hirotaka Noda, [ID] [b] Yunzi Xin, [ID] [b] Hiroki Hasegawa, [ID] [b] Chika Takai, [ID] [b] Takashi Shirai [ID] *[b] and Masayoshi Fuji [ID] [b]

Metal oxides with an oxidation number lower than the highest often exhibit attractive functional properties. However, conventional chemical or thermal reduction of the stable oxides is often laborious and cannot be stopped at an appropriate level of reduction. Therefore, we here try to explore non-conventional reduction processes in a solid-state without external heating. Unique features of reduction processes of SiO_2 toward suboxides, SiO_x ($1 \le x < 2$), were made possible by milling fumed silica nanoparticles with polyolefins (POL), i.e., polypropylene (PP) or polyethylene (PE) and a fluorine-containing one, polyvinylidene difluoride (PVDF). We mainly examined the electronic and coordination states of Si by Si2p XPS spectra and ^{29}Si MAS NMR, respectively. They significantly differ from a similar commercial product obtained via a thermal route. Judging from the chemical shift of ^{29}Si MAS NMR as a criterion of the degree of reduction of SiO_2, the function of POL as a reductant is in the order PP $\approx$ PE > PVDF. Since the present solid-state reaction is free from the formation of unstable gaseous SiO as an intermediate, the products are free from the Si component in a Q^0 state close to that of metallic Si. From these results we conclude that the present silicon suboxides obtained by co-milling silica with POL are closer to those defined as a random bonding model of SiO, than a random mixture model, the former being unachievable by a thermal process. The main mechanism of the present solid-state reduction is the oxygen abstraction from the SiO_4 units by the polarized POL, with its simultaneous oxidative decomposition up to the state of carbon. The reaction process is simple and scalable so that it may offer a new affordable fabrication method of silicon suboxides.

Introduction

Silicon suboxides, SiO_x ($1 \le x < 2$), including nominal SiO, gather increasing interests in view of their diverse application potentials, e.g. coating materials for anti-reflection,[1–3] photo-luminescence[4,5] or anode materials for Li ion batteries.[6–9] SiO_x is usually prepared via a thermal reduction of SiO_2,[10,11] although oxidation of Si metal is also explored as a minor option.[12,13] Associated research works have been predominantly motivated by semiconductor technology.[14,15]

Reduction of silica is already engineered for semiconductor, industrial or solar grade Si.[16,17] Therefore, it seems possible to obtain SiO_x with varying x as an appropriate intermediate stage. However, to stop the thermal reduction process at a desired stage is not so easy. It is generally recognized that gaseous SiO is formed by heating to temperatures up to 2000 K, followed by its condensation. Cooling of SiO is accompanied by its disproportionation to Si and SiO_2.[18–20] An example of a typical fabrication method via a thermal route is heating a mixture of Si and SiO_2 at 1400 °C to obtain gaseous SiO and subsequently condensing at 600 °C.[20] The kinetic process of the disproportionation is dominated by many parameters among others the rate of quenching, including the distance from the heat source and the substrate or the collecting vessel, and hence, difficult to bring under precision control.

Therefore, the stoichiometry, crystallography and microstructure of the nominal SiO are not uniquely defined and remain controversial.[11] There have been some doubts regarding the phase purity of nominal, commercial SiO.[21] Hohl et al.[20] elaborated the structure determination of amorphous SiO in detail and concluded that it is a mixture of nanoclusters of Si dispersed in the matrix comprising SiO_2 or slightly reduced silica. Their conclusions were confirmed by different researchers as well.[22,23]

We therefore try in this study to reduce SiO_2 via an alternative route without passing through the gaseous SiO. We thought it could be done in a solid-state process by milling SiO_2 nanoparticles with solid polyolefin (POL) species. The

[a]Faculty of Science and Technology, Keio University, Yokohama, Japan. E-mail: senna@applc.keio.ac.jp

[b]Advanced Ceramics Research Center, Nagoya Institute of Technology, Tajimi, Japan. E-mail: shirai@nitech.ac.jp

idea is based on our recent findings, that the co-milling of a mixture of metal oxide nanoparticles and hydrocarbon-containing polymers results in the oxidative decomposition of polymers with simultaneous reduction of the oxides and anion exchange, when the POL contains anionic species other than oxygen.[24,25] Hitherto, we preferentially examined TiO_2 and SnO_2 with fluorine-containing hydrocarbons without external or subsequent heating.

Mechanochemical reduction of a complex oxide like magnesium ferrite was worked out in terms of milling media, whereby the stainless-steel media have supposedly played a role of reductant.[26,27] A redox reaction between dissimilar oxides, *e.g.* between α-Fe_2O_3 and SnO, also takes place mechanochemically.[28] These mechanochemical reduction processes were between oxides or oxides and metals. What we are going to discuss in this work, in contrast, deals with those between metal oxides and hydrocarbon species serving as reductants.

Our explicit objectives in this study are to elucidate the process of reducing SiO_2 to SiO_x *via* a solid-state route by co-milling with a POL and to compare the products with commercial SiO as an example of the thermal reduction product. Emphasis is laid on the difference in the electronic and coordination states of Si between the products of mechanochemical and thermal processes by using XPS and ^{29}Si MAS NMR as main analytical tools.

Experimental

Sample preparation

Amorphous pyrogenic (fumed) silica (Aerosil 200, Evonik) without any surface modification was used as a source of SiO_2. Following 3 POL species were chosen as partners of co-milling: polypropylene, PP (IUPAC name, poly(1-methylethylene)), (Seishin Enterprise, PPW-5); polyethylene, PE (IUPAC name, poly(methylene)), (Seishin Enterprise, SK-PE-20L) and a fluorine containing POL, polyvinylidene difluoride, PVDF (IUPAC name poly(1,1-difluoroethylene)), (Aldrich). All the POLs were used as supplied, without pre-treatment. A nominal SiO, supplied by Osaka Titanium (SiO powder, purity 99.95%), fabricated *via* a thermal route, was used for comparison.

Co-milling was carried out by a planetary mill (Fritsch Pulverisette 6) at 300 rpm for up to 3 h. A vial of 80 mL and 15 mm and 5 mm balls, 6 pieces each, were used for milling. All these parts were made of yttria stabilized zirconia, YSZ. The staring mixture comprised silica and POL, with the weight ratio 9 : 1, and the total mass 2.0 g. We will denote those co-milled products henceforth as OXM.

Characterization

The long-range ordering of the products was examined by X-ray diffractometry (XRD, Rigaku MultiFlex). Vibrational spectroscopy *i.e.* Fourier transform infrared spectroscopy (FT-IR, JASCO FT/IR 6200, KBr disk in N2) and Raman scattering spectroscopy (Jasco, NRS-3100 spectrometer with an incident

laser beam of 532.0 nm), were performed to characterize the short-range atomic interaction.

Chemical states of each atomic species were monitored mainly by X-ray photoelectron spectroscopy (XPS, ULVAC-PHI5000 Versa Prove). Si2p and O1s signals were obtained by using a monochromated AlKα beam (1486.6 eV, 25 W), with a spot diameter 100 μm. Calibration of the binding energy was based on the C1s signals on the sample of commercial SiO.

The coordination states of Si were examined by magic angle spinning nuclear magnetic resonance spectroscopy (MAS NMR, VARIAN INOVA-400 plus, PDMS) for ^{29}Si nuclear species. Details of NMR measurement are as follows; offset: 0 ppm, sweep: 500 ppm, scans: 256, acquisition time: 17.2 ms, resolution: 58.2 Hz, observed angle 90 deg: observed width 90: 13 μs × 90, amp. pulse: 100%, and relaxation delay: 120 s. The chemical shift was expressed with a reference of poly-dimethylsiloxane (PDMS), −34.44 ppm.

Color change was observed by diffuse reflectance spectroscopy (UV-vis DRS, Shimadzu, UV-3150). Morphology and fine structures were observed by a field emission scanning electron microscope (FE-SEM: JEOL, JSM-7600F).

Results and discussion

Apparent reduction of silica by co-milling with POL

To examine whether and to what extent silica was reduced by OXM, we first observed O1s XPS spectrum. The results are summarized in Fig. 1. From the spectrum of the starting SiO_2, we observe a single peak at around 533 eV, which was established as that of pure silica.[29] Nominal SiO exhibits also a single peak at around 532.2 eV. Lower binding energy of O1s is a clear indication of reduction of silicon oxides.[30]

The decrease in the O1s binding energy from that of intact silica was also observed by OXM. In the case of PP and PE as POL, peak position is close to that of commercial SiO, but the binding energy is slightly larger than that of SiO. In the case of PVDF, the redshift of the O1s peak is much larger, due to coexisting fluorine, which will be discussed later. From those O1s XPS spectrum, reduction of SiO_2 by OXM is evident.
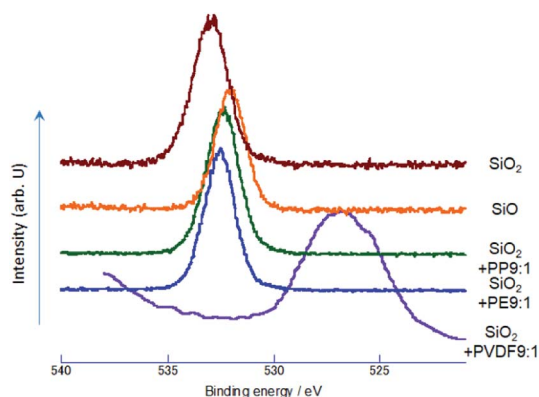

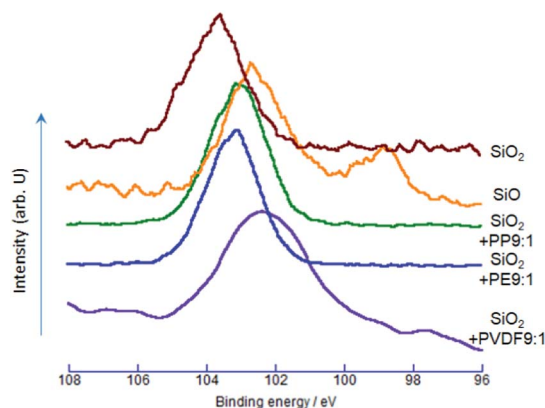**Fig. 1** XPS spectra (O1s) of SiO_2, SiO and the mixtures with SiO_2:POL after milling for 3 h.

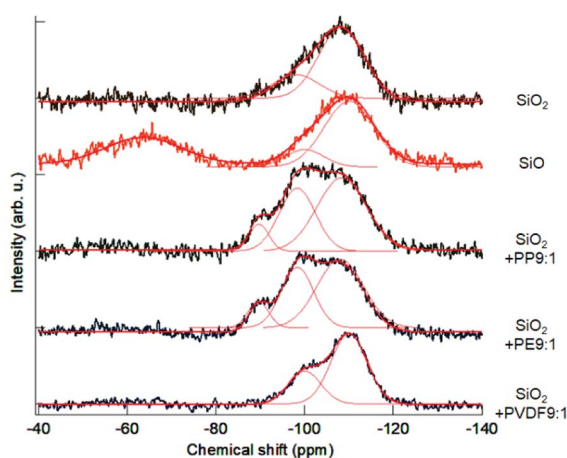**Fig. 2** XPS spectra (Si2p) of SiO₂, SiO and the mixtures with SiO₂:POL after milling for 3 h.

Fig. 3 ²⁹Si MAS NMR spectra of SiO₂, SiO and the mixtures with SiO₂:POL after milling for 3 h.

Electronic states of Si

Change in the electronic states of silicon was examined by Si2p XPS spectra. As shown in Fig. 2, the Si2p binding energy of SiO₂ was at around 103.7 eV, matching well with the literature.[31,32] For the OXM products, the Si2p peaks consistently decreased from that of SiO₂. The decrease in the Si2p binding energy indicates the increase in the electron density around Si, and hence, reduction of silicon from its nominal state of Si^{4+} to lower oxidation states. The decrease in the binding energy is more substantial with PVDF. We think the larger shift by PVDF for the same reason with O1s, although the difference in the

binding energy between PVDF and other POLs of Si2p is not so large as those of O1s.

The most remarkable difference in the spectra between the samples *via* OXM and the commercial SiO is the bimodality of the spectrum of the latter. The peak at around 98.4 eV is very close to those ascribed to the $Si2p_{3/2}$ of metallic silicon.[33,34] The other peak, at around 102.7 eV, corresponds to a slightly reduced state of silicon from that of SiO₂.[31] This quasi two-phase state of nominal SiO will be discussed below in detail.

Change in the coordination states of Si

The profiles of ²⁹Si MAS NMR spectra are shown in Fig. 3. The spectrum of the starting, intact fumed silica exhibited a simple spectrum peak at around −108 ppm, ascribed to Q^4 from $Si(O_4)$.[20,35] Commercial SiO, on the other hand, exhibits two distinct peaks, *i.e.* one close to Q^4 of silica and the other, peaked at around −65 ppm ascribed to Q^0.[20,35] The OXM products exhibited broad peaks ranging between −120 ppm and −80 ppm. We tried to deconvolute these peaks to examine the change in the coordination states of silica, in terms of the relative intensities of Q^n ($1 \leq n \leq 4$), representing the states of $Si(O_n)$. The results are summarized in Table 1.

Intact silica already contains *ca.* 25% of Q^3 state. This is not surprising because of its amorphous and nanocrystalline feature with significant amount of broken Q^4 networks associated with the dangling bonds, particularly in the near surface region. In the commercial SiO, the percentage of Q^4 state is slightly higher. Note that the portion of Q^0 state in the result of SiO was excluded from Table 1. The OXM products exhibit significant amounts of Q^3 and Q^2 states at the cost of the Q^4 contribution. This is a clear indication of loss of oxygen atoms from Q^4 units. Among 3 POL species, PP and PE showed similar proportions of Q^n states. For the OXM treatments with PVDF, the portion of Q^3 is smaller than other two POLs, and Q^2 states was not detected.

Although information of Si2p XPS and ²⁹Si MAS NMR are entirely different from each other, spectral bimodality of commercial SiO is common to both spectra. From these observations, we may safely conclude that the usual, commercially available SiO as a thermal reduction product, consists of two distinct components. One is close to SiO₂ with possible partial loss of oxygen and the other to metallic Si, as frequently claimed in the literature.[20,23,36] Atomic level structure of SiO was interpreted by two different models.[20] A random mixture, comprising nanoparticles of Si dispersed in a silica matric, and a random bonding, where continuous random network comprising $Si_{4-x}O_x$ units is postulated.[20] From the observations

Table 1 Relative intensities (chemical shift) of ²⁹Si MAS NMR signals with different coordination states

Sample/coordination state	Q^1	Q^2	Q^3	Q^4
Intact SiO₂	0	0	25.29 (98 ppm)	74.71 (108 ppm)
Commercial SiO	0	0	16.74 (100 ppm)	83.26 (110 ppm)
Co-milled with PP	0	8.16 (90 ppm)	35.49 (98 ppm)	56.35 (108 ppm)
Co-milled with PE	0	9.48 (90 ppm)	34.49 (98 ppm)	56.03 (108 ppm)
Co-milled with PVDF	0	0	29.74 (100 ppm)	70.25 (110 ppm)

mentioned above, we think the product of OXM is closer to the random bonding model[23,37,38] rather than to the random mixture model.[20,39] It is reported that the former model is stabilized under high pressure,[23] which is actualized during milling as in the present case.

Correlation with vibrational spectroscopy

The FTIR spectra of the co-milled samples and commercial SiO and SiO_2 are shown in Fig. 4. The commercial SiO exhibits a shallow but unique absorption peak at around 590–600 cm^{-1}. This is an absorption band of Si, as reported in the literature, examined in the interests of silicon as a window material of IR spectroscopy.[40] The largest peak is Si–O–Si stretching band at around 1100 cm^{-1} (ref. 41) shifted to a lower wave number by OXM. Note that the degree of the red-shift is different, depending on the POL species. The correlation between the decreases in the Si–O–Si vibrational energy and the O1s binding energy is demonstrated in Fig. 5, including the intact SiO_2 and

Fig. 4 FT-IR spectra of the mixtures with SiO_2:POL.

Fig. 5 Correlation between FT-IR absorption and O1s XPS peaks.

commercial SiO. The observed simple correlation could be interpreted in terms of SiO_2 reduction, accompanied by the increase in the electron density around O^{2-} and consequent retardation of Si–O–Si stretching vibration. Despite the observed clear difference in the reduction mechanisms between thermal and mechanochemical routes, Si–O–Si bending bands at around 450 cm^{-1} and 800 cm^{-1} (ref. 41) are less sensitive to the sample preparation history. Note that we excluded the data with PVDF. The reason will be discussed below.

Comparison of reducing capabilities among 3 POLs

Among three OXM products, the peak shape in the broad range between around 90 ppm and 120 ppm are significantly different from those of SiO. From the literature, we may assign the peak at around −100 ppm to Q^3 and −90 ppm to Q^2.[42–45] We also note that no significant signal appeared in this range from the commercial SiO.

As already discussed by referring Table 1, the states of the OXM products with PP and PE are similar. The percentage of Q^4 is significantly larger with PVDF than PP and PE, indicating the smaller ability of PVDF for mechanochemical reduction. We observe no significant difference in the peak position from SiO_2 and SiO at around −108 to −110 ppm, unlike the case of XPS spectra, where the difference of the peak positions of both O1s and Si2p was more significant. This again suggest the difference in the states of Si after thermal and mechanochemical treatments. In the actual OXM process, C–H bonds in olefins are close neighbor to the OXM products and hence they are most probably polarized,[46] favoring the oxygen abstraction. Similar view was extensively discussed in the interests of catalytic oxidation of hydrocarbons,[47,48] although our experimental results were not extended to examine the extent of polarization.

We also point out that the co-milled sample with PVDF was excluded from Fig. 5, as its properties were widely apart from the other samples, as we already noticed from O1s XPS spectra (Fig. 2). This again must be attributed to the coexistence of fluorine. Researchers in the field of semiconductor etching report that fluorine is a powerful disrupter of silica-based compounds.[49–51] While the related process is conventionally practiced in liquid[52] or vapor[53] phases, same principles could be applicable in the solid phase. Decrease in the O1s binding energy is closely correlated with decreasing interaction parameter of cation and anion of many metal oxides,[54] which, in turn, parallels to the polarizability.[55] Incorporation of the chemical species with high polarizability like fluorine reduces the interaction parameter and hence O1s binding energy, although more exact discussion on this point is yet to be done.

States of POL after milling

After co-milling SiO_2 with POL, we observed darkening of the sample color (ESI, Fig. S1†). The UV-vis diffuse reflectance spectra are shown in Fig. 6. We observed black dots in the co-milled products with PVDF or PP under scanning electron microscope (Fig. S2 and S3†). Since the micrographs alone cannot determine that the darkening is attributed to the
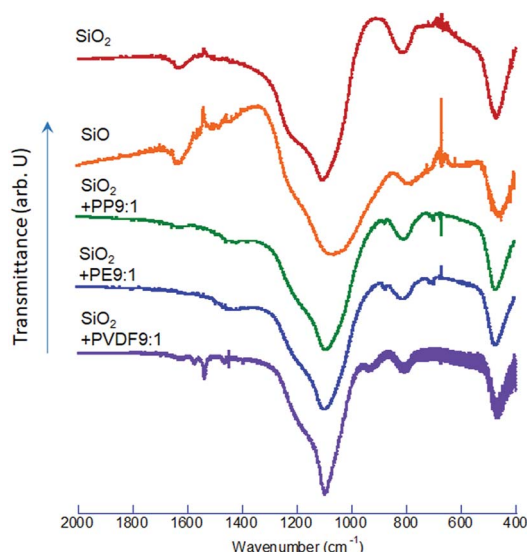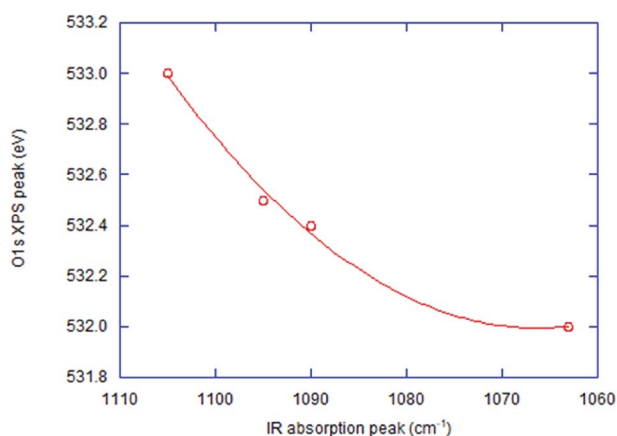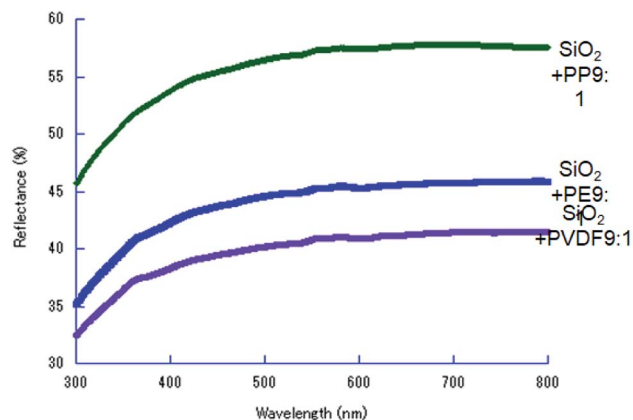
Fig. 6 UV-vis DRS of the co-milled products.

Fig. 8 XRD of PP, PE and PVDF co-milled with SiO_2. Arrows denote c–ZrO_2 (JCPDS-27-0997).
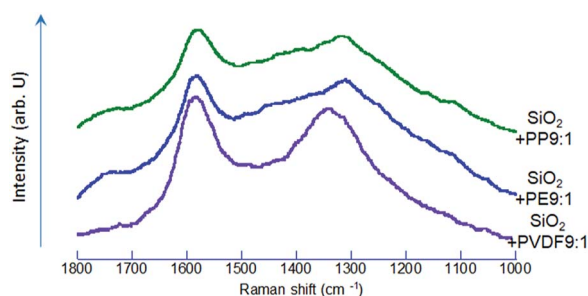

Fig. 7 Raman spectra of the mixtures with SiO_2:POL after milling for 3 h.

formation of carbon particles, we examined these samples by Raman spectroscopy.

As shown in Fig. 7, the Raman spectra exhibit typical G and D peaks. The former is derived from "graphite", observed at around 1550–1600 cm^{-1}, and represents the in-plane bond-stretching vibration of a pair of sp^2 carbon atoms in E_{2g} symmetry. The D peak, derived from "disorder", at around 1350 cm^{-1}, is ascribed to the breathing vibration in A_{1g} symmetry.[56] This indicates that the carbon species, preferentially in a sp^2 state, were formed[57] by co-milling. This indicates that the oxidative decomposition of POL was proceeded up to the state of carbonization.

Changes in the crystallographic properties

The nominal solid compound, SiO, is understood to be metastable and amorphous,[22] with a unique interfacial nanostructure.[20] Although there are some reports mentioning the crystalline SiO,[10] the metastable, amorphous states were supported by computer simulation as well.[23] The XRD profiles shown in Fig. 8 exhibit only hallo pattern, except relatively sharp peaks of cubic ZrO_2, indicated by the arrows, from the milling balls and vessel. We note that the intensity of the ZrO_2 diffraction peaks are not identical but depends on POL specie, *i.e.* PP $\approx$ PE $\geq$ PVDF. Incorporation of zirconia into the milled product cannot simply be associated with simple mechanical abrasion, but because of mechanochemical reaction between
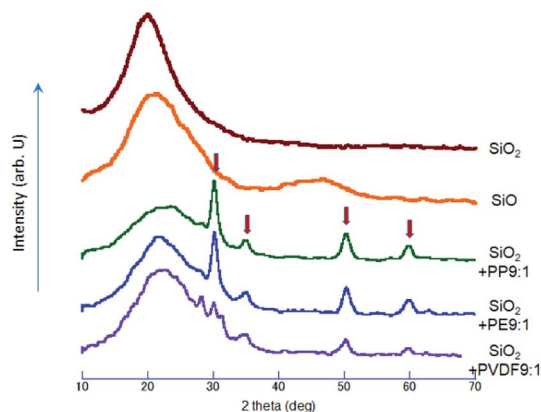
POL and ZrO_2, as we have been suggested with various combination of POL and other oxides, TiO_2 (ref. 24 and 58) and SnO_2.[25] It is to be noted that the sequences of the degree of reduction and the apparent amount of ZrO_2 exhibit qualitative parallelism. This serves as another, independent evidence of the present mechanochemical reduction, to be the result of mechanochemical reaction between silica and POL. A small diffraction peak at around 28 degree two theta, on the curve with PVDF is ascribed to that of PVDF, a part of which is remained as a crystalline state. This is an indication of lesser amount of oxidative decomposition of PVDF as compared to PP and PE, in line with its lesser reducing ability as mentioned above.

Conclusions

The reduction route of SiO_2 toward silicon suboxides, SiO_x ($1 \leq x \leq 2$), by milling fumed silica nanoparticles with polyolefins (POLs), with and without fluorine (OXM process), is distinctly different from conventional thermal route. This was confirmed by Si2p XPS and ^{29}Si MAS NMR by using 3 POL species, *i.e.* poly(propene) (PP), poly(methylene) (PE) or poly(1,1-difluoroethylene) (PVDF) with the corresponding signals from commercial SiO as a reference of the thermally reduced product. We found a good correlation between O1s binding energy observed by XPS and Si–O–Si stretching vibration energy by FTIR, except PVDF, with which, O1s signal has been influenced *via* a different factor due to coexisting fluorine. The change in the coordination states detected by ^{29}Si NMR was significantly smaller by using PVDF than PP and PE. Since the present solid-state reduction does not involve the unstable gaseous SiO as an intermediate, the products are free from Q^0 state close to that of metallic Si. From these results we conclude that the OXM products are closer to those defined as random bonding model of SiO, than a random mixture model, the former a thermal process could not achieve. The main reduction mechanism of OXM is the oxygen abstraction from the SiO_4 units by the polarized POL, with its simultaneous oxidative decomposition up to the state of carbon. The reaction process is simple and scalable so that it may offer a new affordable fabrication method of silicon suboxides.

Conflicts of interest

There are no conflicts to declare.

Acknowledgements

References

1 M. T. K. Soh, N. Savvides, P. J. Martin and C. A. Musca, On the Bonding Microstructure of Amorphous Silicon Oxide Thin Films, *Thin Solid Films*, 2006, **515**, 2284–2290.

2 J.-I. Lee and S. Park, High-Performance Porous Silicon Monoxide Anodes Synthesized Via Metal-Assisted Chemical Etching, *Nano Energy*, 2013, **2**, 146–152.

3 Y. Baba, T. Sekiguchi, I. Shimoyama and N. Hirao, Electronic Structures of Silicon Monoxide Film Probed by X-Ray Absorption Spectroscopy, *Surf. Sci.*, 2013, **612**, 77–81.

4 Y. D. Glinka, S.-H. Lin and Y.-T. Chen, The Photoluminescence from Hydrogen-Related Species in Composites of SiO_2 Nanoparticles, *Appl. Phys. Lett.*, 1999, **75**, 778.

5 D. Nesheva, Photoluminescence from SiO_x Layers Containing Amorphous Silicon Nanoparticles, *Phys. Status Solidi A*, 2012, **209**, 746–751.

6 H. Sepehri-Amin, T. Ohkubo, M. Kodzuka, H. Yamamura, T. Saito, H. Iba and K. Hono, Evidence for Nano-Si Clusters in Amorphous Sio Anode Materials for Rechargeable Li-Ion Batteries, *Scr. Mater.*, 2013, **69**, 92–95.

7 K. W. Kim, H. Park, J. G. Lee, J. Kim, Y.-U. Kim, J. H. Ryu, J. J. Kim and S. M. Oh, Capacity Variation of Carbon-Coated Silicon Monoxide Negative Electrode for Lithium-Ion Batteries, *Electrochim. Acta*, 2013, **103**, 226–230.

8 Y. Hwa, C.-M. Park and H.-J. Sohn, Modified Sio as a High Performance Anode for Li-Ion Batteries, *J. Power Sources*, 2013, **222**, 129–134.

9 J. K. Lee, W. Y. Yoon and B. K. Kim, Kinetics of Reaction Products of Silicon Monoxide with Controlled Amount of Li-Ion Insertion at Various Current Densities for Li-Ion Batteries, *J. Electrochem. Soc.*, 2014, **161**, A927–A933.

10 B. G. Gribov, K. V. Zinov'ev, O. N. Kalashnik, N. N. Gerasimenko, D. I. Smirnov and V. N. Sukhanov, Structure and Phase Composition of Silicon Monoxide, *Semiconductors*, 2012, **46**, 1576–1579.

11 X. Li, G. Zhang, R. Tronstad and O. Ostrovski, Reduction of Quartz to Silicon Monoxide by Methane-Hydrogen Mixtures, *Metall. Mater. Trans. B*, 2016, **47**, 2197–2204.

12 M. Tagawa, T. Emma, H. Kinishita, N. Ohmae, M. Umeno and T. K. Mintoni, Formation of Thin Oxide Films on Room-Temperature Silicon (100) by Exposure to a Neutral Beam of Hyperthermal Atomic and Molecular Oxygen, *Jpn. J. Appl. Phys.*, 1998, **37**, L1455–L1457.

13 M. Y. Bashouti, K. Sardashti, J. Ristein and S. Christiansen, Kinetic Study of H-Terminated Silicon Nanowires Oxidation in Very First Stages, *Nanoscale Res. Lett.*, 2013, **8**, 41.

14 E. San Andrés, A. del Prado, I. Mártil, G. González-Díaz and F. L. Martínez, Rapid Thermal Annealing Effects on the Electrical Behavior of Plasma Oxidized Silicon/Silicon Nitride Stacks Gate Insulators, *J. Vac. Sci. Technol., B: Microelectron. Nanometer Struct.*, 2003, **21**, 1306–1313.

15 G. Aygun and I. Yildiz, Interfacial and Structural Properties of Sputtered HfO_2 Layers, *J. Appl. Phys.*, 2009, **106**, 014312.

16 G. del Coso, C. del Cañizo and W. C. Sinke, The Impact of Silicon Feedstock on the Pv Module Cost, *Sol. Energy Mater. Sol. Cells*, 2010, **94**, 345–349.

17 P. G. Loutsenhiser, O. Tuerk and A. Steinfeld, Production of Si by Vacuum Carbothermal Reduction of SiO_2 Using Concentrated Solar Energy, *JOM*, 2010, **62**, 49–54.

18 J. A. Nuth and F. T. Ferguson, Silicates Do Nucleate in Oxygen-Rich Circumstellar Outflows: New Vapor Pressure Data for SiO, *Astrophys. J.*, 2006, **649**, 1178–1183.

19 A. Samanta and D. Das, Studies on the Structural Properties of SiO:H Films Prepared from (SiH_4+CO_2+He) Plasma in Rf-Pecvd, *Sol. Energy Mater. Sol. Cells*, 2009, **93**, 588–596.

20 A. Hohl, T. Wieder, P. A. van Aken, T. E. Weirich, G. Denninger, M. Vidal, S. Oswald, C. Deneke, J. Mayer and H. Fuess, An Interface Clusters Mixture Model for the Structure of Amorphous Silicon Monoxide (Sio), *J. Non-Cryst. Solids*, 2003, **320**, 255–280.

21 B. Friede and M. Jansen, Some Comments on So-Called Silicon Monoxide, *J. Non-Cryst. Solids*, 1996, **204**, 202–203.

22 S. M. Schnurre, J. Gröbner and R. Schmid-Fetzer, Thermodynamics and Phase Stability in the Si–O System, *J. Non-Cryst. Solids*, 2004, **336**, 1–25.

23 K. AlKaabi, D. L. Prasad, P. Kroll, N. W. Ashcroft and R. Hoffmann, Silicon Monoxide at 1 Atm and Elevated Pressures: Crystalline or Amorphous?, *J. Am. Chem. Soc.*, 2014, **136**, 3410–3423.

24 M. Senna, V. Šepelák, J. Shi, B. Bauer, A. Feldhoff, V. Laporte and K.-D. Becker, Introduction of Oxygen Vacancies and Fluorine into TiO_2 Nanoparticles by Co-Milling with Ptfe, *J. Solid State Chem.*, 2012, **187**, 51–57.

25 M. Senna, E. Turianicová, V. Šepelák, M. Bruns, G. Scholz, S. Lebedkin, C. Kübel, D. Wang, M. Kaňuchová, M. Kaus and H. Hahn, Fluorine Incorporation into SnO_2 Nanoparticles by Co-Milling with Polyvinylidene Fluoride, *Solid State Sci.*, 2014, **30**, 36–43.

26 M. Menzel, V. Šepelák and K. D. Becker, Mechanochemical Reduction of Nickel Ferrite, *Solid State Ionics*, 2001, **141–142**, 663–669.

27 V. Šepelák, M. Menzel, K. D. Becker and F. Krumeich, Mechanochemical Reduction of Magnesium Ferrite, *J. Phys. Chem. B*, 2002, **106**, 6672–6678.

28 V. Šepelák, M. J. Nasr Isfahani, M. Myndyk, M. Ghafari, A. Feldhoff and K. D. Becker, Complementary [57]fe and [119]sn Mössbauer Study of Mechanochemical Redox Reaction, *Hyperfine Interact.*, 2011, **202**, 39–46.

29 H. J. M. Bosman, A. P. Pijpers and A. W. M. A. Jaspers, An X-Ray Photoelectron Spectroscopy Study of the Acidity of SiO_2–ZrO_2 Mixed Oxides, *J. Catal.*, 1996, **161**, 551–559.

30 G. Aygun, E. Atanassova, K. Kostov and R. Turan, Xps Study of Pulsed Nd:Yag Laser Oxidized Si, *J. Non-Cryst. Solids*, 2006, **352**, 3134–3139.

31 H. Takezawa, K. Iwamoto, S. Ito and H. Yoshizawa, Electrochemical Behaviors of Nonstoichiometric Silicon Suboxides (Siox) Film Prepared by Reactive Evaporation for Lithium Rechargeable Batteries, *J. Power Sources*, 2013, **244**, 149–157.

32 B. Ulgut and S. Suzer, Xps Studies of SiO_2/Si System under External Bias, *J. Phys. Chem. B*, 2003, **107**, 2939–2943.

33 W. E. Morgan and J. R. Van Wazer, Binding Energy Shifts in the X-Ray Photoelectron Spectra of a Series of Related Group Iv-a Compounds, *J. Phys. Chem.*, 1973, **77**, 964–969.

34 N. Srivastava, T. Shripathi and P. C. Srivastava, Core Level X-Ray Photoelectron Spectroscopy Study of Exchange Coupled Fe/Nio Bilayer Interfaced with Si Substrate (Fe/Nio–Nsi Structure), *J. Electron Spectrosc. Relat. Phenom.*, 2013, **191**, 20–26.

35 R. H. Glaser and G. L. Wilkes, Solid-State ^{29}Si NMR of TEOS-Based Multifunctional Sol-Gel Materials, *J. Non-Cryst. Solids*, 1989, **113**, 73–87.

36 C.-M. Park, W. Choi, Y. Hwa, J.-H. Kim, G. Jeong and H.-J. Sohn, Characterizations and Electrochemical Behaviors of Disproportionated SiO and Its Composite for Rechargeable Li-Ion Batteries, *J. Mater. Chem.*, 2010, **20**, 4854.

37 T. P. Nguyen and S. Lefrant, Xps Study of SiO Thin Films and SiO-Metal Interface, *J. Phys.: Condens. Matter*, 1989, **1**, 5197–5204.

38 A. Barranco, F. Yubero, J. P. Espinós, P. Groening and A. R. González-Elipe, Electronic State Characterization of Siox Thin Films Prepared by Evaporation, *J. Appl. Phys.*, 2005, **97**, 113714.

39 K. Schulmeister and W. Mader, Tem Investigation on the Structure of Amorphous Silicon Monoxide, *J. Non-Cryst. Solids*, 2003, **320**, 143–150.

40 M. Song, T. H. Kim, M. S. Hyun, J. H. Park and H. Y. Kim, Study on Optimizing the Thickness of Silicon Window of Wlp for Ir Sensor, *Proc. SPIE*, 2012, **8353**, 83532B.

41 E. M. Valliant, C. A. Turdean-Ionescu, J. V. Hanna, M. E. Smith and J. R. Jones, Role of Ph and Temperature on Silica Network Formation and Calcium Incorporation into Sol–Gel Derived Bioactive Glasses, *J. Mater. Chem.*, 2012, **22**, 1613–1619.

42 E. Lippmaa, M. Magi, A. Samoson, G. Engelharld and A. R. Grimmer, Structural Studies of Silicates by Solid-State High Resolution ^{29}Si NMR, *J. Am. Chem. Soc.*, 1980, **102**, 4889–4893.

43 M. Mägi, E. Lippmaa and A. Samoson, Solid-State High-Resolution Silicon-29 Chemical Shifts in Silicates, *J. Phys. Chem.*, 1984, **88**, 1518–1522.

44 G. Engelhardt, H. Jancke, E. Lippmaa and A. Samoson, Structure Investigations of Solid Organosilicon Polzmers Bz High Resolution Solidaßstate Nmr, *J. Organomet. Chem.*, 1981, **219**, 295–301.

45 R. Dupree, D. Holland and D. S. Williams, An Assessment of the Structural Models for Amorphous SiO Using Mas Nmr, *Philos. Mag. B*, 1984, **50**, L13–L18.

46 G. Busca, V. Lorenzelli, G. Ramis and V. S. Escribano, Chemistry of Olefins at Metal Oxide Surfaces: A Tool for Surface Science of Oxide Catalysts, *Mater. Chem. Phys.*, 1991, **29**, 175–189.

47 R. J. Gritter, G. D. Dupre and T. J. Wallace, Oxidation of Benzyl Alcohols with Manganese Oxide, *Nature*, 1964, **4928**, 179–181.

48 Y. Meng, H. C. Genuino, C. H. Kuo, H. Huang, S. Y. Chen, L. Zhang, A. Rossi and S. L. Suib, One-Step Hydrothermal Synthesis of Manganese-Containing Mfi-Type Zeolite, Mn-ZSM-5, Characterization, and Catalytic Oxidation of Hydrocarbons, *J. Am. Chem. Soc.*, 2013, **135**, 8594–8605.

49 K. Awazu, Fluorinated Silica Glass Ablated with Arf Excimer Laser at Low Fluence, *J. Non-Cryst. Solids*, 2007, **353**, 215–217.

50 Z. Luo, W. Liu, G. Qu, A. Lu and G. Han, Sintering Behavior, Microstructure and Mechanical Properties of Various Fluorine-Containing Y-Sialon Glass-Ceramics, *J. Non-Cryst. Solids*, 2014, **388**, 62–67.

51 D. H. Lee, S. J. Choo, U. Jung, K. W. Lee, K. W. Kim and J. H. Park, Low-Loss Silicon Waveguides with Sidewall Roughness Reduction Using a Sio2 hard Mask and Fluorine-Based Dry Etching, *J. Micromech. Microeng.*, 2015, **25**, 015003.

52 H. Ye, Y. Li, Z. Yuan and Q. Zhang, Ultrasonic-Assisted Wet Chemical Etching of Fused Silica for High-Power Laser Systems, *Int. J. Appl. Glass Sci.*, 2018, **9**, 288–295.

53 F. Venturini, M. Sansotera, R. M. Vazquez, R. Osellame, G. Cerullo and W. Navarrini, Micromanufacturing in Fused Silica Via Femtosecond Laser Irradiation Followed by Gas-Phase Chemical Etching, *Micromachines*, 2012, **3**, 604–614.

54 V. Dimitrov and T. Komatsu, Effect of Interionic Interaction on the Electronic Polarizability, Optical Basicity and Binding Energy of Simple Oxides, *J. Ceram. Soc. Jpn.*, 1999, **107**, 1012–1018.

55 J. R. Tessman, A. H. Kahn and W. Shockley, Electronic Polarizabilities of Ions in Crystals, *Phys. Rev.*, 1953, **92**, 890–895.

56 A. C. Ferrari, S. E. Rodi and J. Robertson, Interpretation of Infrared and Raman Spectra of Amorphous Carbon Nitrides, *Phys. Rev. B: Condens. Matter Mater. Phys.*, 2003, **67**, 155306.

57 V. N. Tsaneva, W. Kwapinski, X. Teng and B. A. Glowacki, Assessment of the Structural Evolution of Carbons from Microwave Plasma Natural Gas Reforming and Biomass Pyrolysis Using Raman Spectroscopy, *Carbon*, 2014, **80**, 617–628.

58 M. Senna, A. Düvel, V. Šepelák, J. Shi, K. L. Da Silva, V. Laporte, S. Lebedkin, C. Kübel, D. Wang, D. Schünemann, K. D. Becker and P. Heitjans, Transfer and State Changes of Fluorine at Polytetrafluoroethylene/Titania Boundaries by Mechanical Stressing and Thermal Annealing, *J. Phys. Chem. C*, 2013, **117**, 15272–15278.